Bzowski *et al. EJNMMI Physics* (2022) 9:41
https://doi.org/10.1186/s40658-022-00471-1

EJNMMI Physics

ORIGINAL RESEARCH

Efficiency of ^{124}I radioisotope production from natural and enriched tellurium dioxide using ^{124}Te(p,xn)^{124}I reaction

Paweł Bzowski[1,2,3], Damian Borys[1,2,3*], Kamil Gorczewski[1], Agnieszka Chmura[4], Kinga Daszewska[4], Izabela Gorczewska[1], Anna Kastelik-Hryniewiecka[4], Marcin Szydło[4], Andrea d'Amico[1] and Maria Sokół[5]

*Correspondence: damian.borys@polsl.pl

[2] Department of Systems Biology and Engineering, Silesian University of Technology, Akademicka 16, 44-100 Gliwice, Poland
Full list of author information is available at the end of the article

Abstract

Background: ^{124}I Iodine ($T_{1/2} = 4.18$ d) is the only long-life positron emitter radioisotope of iodine that may be used for both imaging and therapy as well as for ^{131}I dosimetry. Its physical characteristics permits taking advantages of the higher Positron Emission Tomography (PET) image quality, whereas the availability of new molecules to be targeted with ^{124}I makes it a novel innovative radiotracer probe for a specific molecular targeting.

Results: In this study Monte Carlo and SRIM/TRIM modelling was applied to predict the nuclear parameters of the ^{124}I production process in a small medical cyclotron IBA 18/9 Cyclone. The simulation production yields for ^{124}I and the polluting radioisotopes were calculated for the natural and enriched $^{124}TeO_2 + Al_2O_3$ solid targets irradiated with 14.8 MeV protons. The proton beam was degraded energetically from 18 MeV with 0.2 mm Havar foil. The ^{124}Te(p,xn)^{124}I reactions were taken into account in the simulations. The optimal thickness of the target material was calculated using the SRIM/TRIM and Geant4 codes. The results of the simulations were compared with the experimental data obtained for the natural $TeO_2 + Al_2O_3$ target. The dry distillation technique of the 124-iodine was applied.

Conclusions: The experimental efficiency for the natural Te target was better than 41% with an average thick target (>0.8 mm) yield of 1.32 MBq/µAh. Joining the Monte Carlo and experimental approaches makes it possible to optimize the methodology for the ^{124}I production from the expensive Te enriched targets.

Keywords: 124-I, Iodine, Cyclotron, Monte Carlo, Nuclear medicine, Production, Radioisotope, PET-CT

Introduction

Radiotracers used in nuclear medicine diagnostics are substrates of normal physiological pathways (activated probes) or localize to particular targets because of specific binding interactions (targeted probes) [1]. One of the most prevalent radioisotopes for metabolic imaging and treatment is ^{131}I. It is produced in nuclear reactors and is usually used to diagnose and treat different thyroid diseases. However, the accelerating demands of non-standard PET necessitate development and optimization methods and applications for emerging radionuclides, especially ^{124}I. ^{124}I provides better thyroid diagnostics, delivers less dose to patients and reduces the risk of thyroid stunning [2], facilitating subsequent therapy. Moreover, ^{124}I is an attractive radionuclide for radiolabeling of monoclonal antibodies (mAbs), potential immunoPET imaging pharmaceuticals, due to its physical properties (the decay characteristics and a half-life suitable to study the processes with slow bio-kinetics [3]), typical and routine cyclotron production protocols, and well-established methodologies for radioiodination [4]. However, the practical implementation of ^{124}I production in cyclotrons requires adapting the device configuration to the chosen production methodology but is highly supported by the EANM organisation [5].

^{124}I has dual energy emission: beta radiation emissions of 1532 keV (11%) and 2135 keV (11%) and gamma emissions of 511 keV (46%), 603 keV (61%), and 1691 keV (11%). The gamma constant is 2.05E-4 mSv/hr per MBq @ 1.0 meter. The physical half-time ($T_{1/2}$) of ^{124}I is 4.18 days, its biological half-time is 120–138 days, and the effective half-time equals 4 days [6]. The intake routes for ^{124}I may be ingestion, inhalation, puncture, wound or skin contamination and the radiotoxicity differs if the ^{124}I is ingested (2.82E-7 Sv/Bq) or inhaled (1.69E-7 Sv/Bq) [6–8].

Several routes can be used to produce ^{124}I in cyclotron—the choice of the strategy depends on the availability of irradiating particles and their energy ranges at a particular facility [9, 10]. One of the first schemes has been based on ^{124}Te via the ^{124}Te(d,2n)^{124}I reaction [11–15]. In recent years ^{124}I is produced from $^{124}TeO_2$ via the reaction ^{124}Te(p,n)^{124}I [16–19]. This reaction has the advantages of using cyclotrons with the proton energies lower than 14 MeV, providing high radionuclidic purity, but its yields are rather low, being between roughly 6 and 20 MBq/μAh, depending on the effective energy range and the target composition [9, 20].

In this study, Geant4 (GEometry ANd Tracking 4) Monte Carlo simulation toolkit [21–23] was utilized. Geant4 is a toolkit for simulating the passage of particles through matter, and its functionalities include tracking, geometry, physics models and hits. In this environment, we calculated the proton beam penetration within the modelled target and compared the results with those from SRIM/TRIM software by Ziegler [24]. The model proposed by Poignant et al. [25] was used to optimize the production prerequisites of ^{124}I via ^{124}Te(p, n)^{124}I reaction and its co-produced impurities. However, the parameters of the model were modified—the GE PETtrace cyclotron geometry was changed to reflect the geometry appropriate for IBA 18/9 Cyclone Cyclotron with Solid Target capabilities. The experimental data from the ^{124}I production in IBA 18/9 Cyclone cyclotron and using Nitra Solid State Target were compared with the semi-experimental results from the process modelling. The aim was to adapt the production methodology of ^{124}I to small medical cyclotrons and to optimize the types and thicknesses of degradation foils and target materials. The influence of the proton beam parameters on the production yield of ^{124}I was taken into account.

Materials and methods

This work consists of the semi-empirical Monte Carlo simulations and the empirical approach involving the experimental production of ^{124}I from the natural Tellurium Dioxide (>99% purity, MERCK company). The workflow diagram is presented in Fig. 1.

In the experiment IBA 18/9 Cyclone cyclotron (a nominal energy of 18 MeV) installed at Maria Sklodowska-Curie National Research Institute of Oncology Gliwice Branch with a dedicated Nitra Solid COSTIS (manufactured by Elex Commerce) target for a solid material irradiation was employed.

Geant4 toolkit was applied for simulating the ^{124}I production from the natural and enriched TeO_2 targets and using various proton energy degrading foils: Havar, Molybdenum and Aluminum, as well as two proton currents: 10 µA and 15 µA. The role of the simulation parameters, such as protons energy, beam current, target material, beam energy degraders, their thicknesses and irradiation time was analyzed and optimized since these are the main sources of systematic errors and cumulative energy shifts. SRIM/TRIM (Stopping and Range of Ions in Matter), a program by Ziegler [24], was also used for validation of the production methods. This program is equipped with a graphical user interface, making the modelling much easier.

Because a sufficiently large number of particles should be simulated and tracked to obtain reasonable results, a computing cluster was used.

Target preparation

The targetry system for production of ^{124}I is limited to solid targets, usually either elemental tellurium or tellurium oxide, but the latter has better thermal characteristics as compared to the former. The natural TeO_2 used in the experiment contains ^{120}Te (0.09%), ^{122}Te (2.55%), ^{123}Te (0.89%), ^{124}Te (4.74%), ^{125}Te (7.07%), ^{126}Te (18.84%), ^{128}Te (31.74%), and ^{130}Te (34.08%) (National Nuclear Decay Center; Brookhaven National Lab. 2009. Available online: http://www.nndc.bnl.gov/).

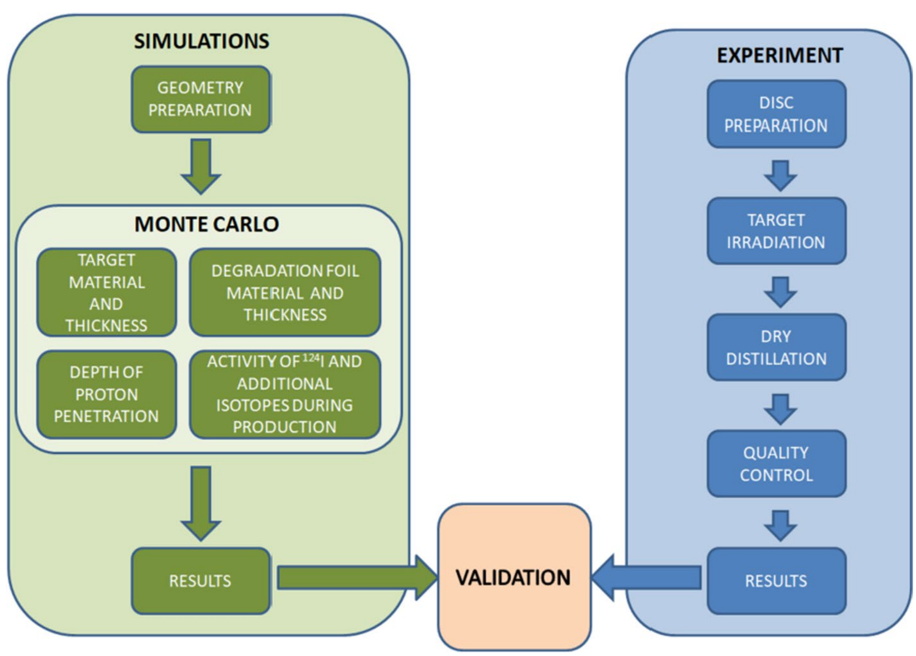

Fig. 1 Flowchart of the Monte Carlo simulations of the ^{124}I production and the production process experimental verification

As a target plate material, platinum was chosen, because of its high thermal conductivity (71.6 W/(m*K)) and high melting temperature (1768 °C). Such properties allow for efficient cooling during the proton beam irradiation and prevent the disc from thermal damage during TeO_2 melting. The Pt disc has a diameter of 24 mm, a thickness of 2 mm and a 1 mm deep, circular cavity of 12 mm in the centre (Fig. 2a).

The production process starts from inserting ca. 400 mg of the $^{124}TeO_2 + Al_2O_3$ mix (5-7wt% of aluminum oxide) into the cavity using the TERIMO module, an automatic module for separation the iodine radionuclides from the irradiated tellurium oxide targets (Fig. 2b). Al_2O_3 serves two purposes: to enhance the adhesion of $^{124}TeO_2$ to the target disk and to produce a glassy solid matrix enhancing the materials structure [26].

The melting of the $^{124}TeO_2 + Al_2O_3$ mix is performed in several stages to reduce the loss of TeO_2. First, the target is annealed at 450 °C to convert a small amount of TeO_3 (which occasionally occurs in TeO_2) to TeO_2 [9]. Then, the temperature is increased up to the melting point of tellurium dioxide (733 °C) and kept for 10–20 min. After that, the mixture inside the metal disc is cooled slowly, and a glassy layer is formed, which is stuck to Pt (Fig. 3a). The tellurium dioxide glass density is 5.65 g/cm^3 [27, 28]. In the experiments, the melted tellurium dioxide weight within the cavity was ca. 400 mg; the filled cavity depth was ca. 0.6 mm, and the volume of the material was 0.07 cm^3.

It is essential to optimize the amount of material on the disc. The Monte Carlo computing significantly shorten the optimization time yielding the optimal geometry and the thickness of the $^{124}TeO_2$ layer.

Target irradiation

During the bombardment, the target material was cooled with a recirculating chilled helium gas stream (gas pressure: 0.5 MPa) directed at the target, while the target holder backing was water-cooled on the front and a water flow of 16 L/min on the platinum backing. The nominal cyclotron energy of 18 MeV was moderated with a degrading foil: Havar, Molybdenum or Aluminum were applied in the simulations, whereas the experiments were performed using 0.2 mm Havar. At 14 MeV the cross-section for ^{124}I is ca. 300 mb, whereas for 18 MeV it is three times lower [20, 29]. At this stage of the experiment, the proper choice of a proton beam current and a target irradiation time is crucial for production efficiency. If these parameters are too low, the amount of the produced

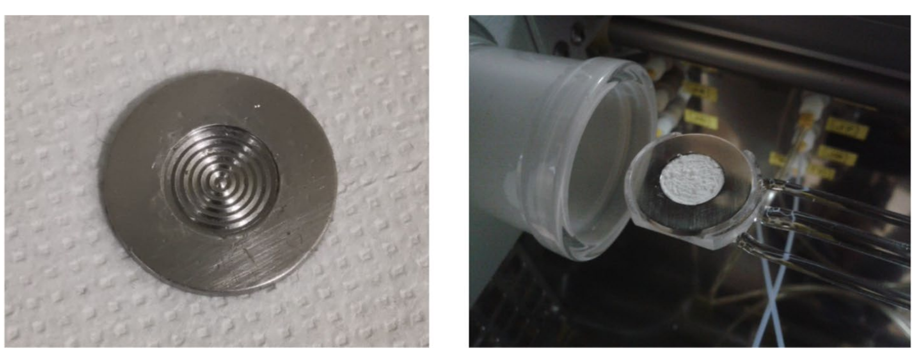

(a) Empty platinum disc. (b) Disc filled with $TeO_2 + Al_2O_3$.

Fig. 2 Exemplary empty target disc and target disc filled with TeO_2

(a) Before irradiation. (b) After irradiation.

Fig. 3 Exemplary TeO_2 target disc before (**a**) and after (**b**) irradiation

^{124}I radionuclide is not sufficient, but if they are too high, the target could be overheated and the trapped ^{124}I could leave the disc decreasing the amount of the final product. While the use of TeO_2 targets offers the benefit of re-irradiating the same target, such targets are limited to irradiation currents of typically less than 30 μA and often less than 10 μA [30]. That is why we applied two values from this rage: 10 and 15 μA. They seemed to be safe for the production process. After each irradiation, the target surface became, however, blackened (Fig. 3a, b), which occurs due to the thermal gradients caused by the interaction of protons with the target material.

Dry distillation

A standard separation method of ^{124}I from the TeO_2 target is a dry distillation process. It consists of submitting the heated target material in a quartz tube under a gas flow, which removes the traces of TeO_2 and traps the radioiodine while retaining the target material on the target plate.^{124}I sublimes from the melted tellurium oxide (its melting point is 733 °C).

In the experiment, the process of trapping the released iodine was carried out at 750 °C. In a routine procedure, the gas with ^{124}I is pumped to a solution of NaOH where it cools down and reacts to ^{124}I-NaI. The flow of air transporting the iodine vapours to the NaOH solution was 100 ml/min. The flow rate of the reagents was 350 ml/min, while the transport of the products was set to 250 ml/min. The final product is a solution of ^{124}I-NaI in H_2O.

The separation was performed using the TERIMO reagent vials (B1-B5) dispensing the reagents and the cleaning solutions to the trapping vial and filled as follows:

- B1 : 1ml of NaOH
- B2 : 2ml of H_2O
- B3 : 1ml of NaOH
- B4 : 1ml of H_2O
- B5 : 2ml of H_2O

A typical separation process takes approximately 90 minutes and delivers a ready-to-use product vial. The tellurium target can be used several times as each dry distillation

Table 1 The target masses (with platinum disc) before and after the subsequent three bombardments as well as the corresponding mass losses for the irradiated discs 1 and 2

Disc	N^{O}	Mass before production [g]	Mass after production [g]	ΔMass
1	1	13.2790	13.2750	0.0040
	2	13.2750	13.2712	0.0038
	3	13.2712	13.2678	0.0034
2	1	13.0700	13.0675	0.0025
	2	13.0675	13.0642	0.0033
	3	13.0642	13.0611	0.0031

Table 2 Production efficiency at the end of the separation, the product (P) and waste (W) activities

Beam current [μA]	N^{O}	Activity P [MBq]	Activity W [MBq]	Activity P+W [MBq]	%P	%W
10	1	16.28	4.44	20.72	78.44	21.56
	2	10.36	3.70	14.06	74.12	25.88
	3	13.69	1.11	14.80	93.37	6.63
	4	17.76	0.74	18.50	95.93	4.07
	5	11.84	4.07	15.91	74.33	25.67
	6	17.39	3.33	20.72	83.25	16.75
	7	24.42	0.74	25.16	97.19	2.81
	8	22.20	1.11	23.31	94.79	5.21
	9	12.95	1.48	14.43	90.83	9.17
15	10*	52.17	4.07	56.61	92.59	7.41

The irradiation parameters: beam current 10 μA (N^{O}: 1–9) and 15 μA (N^{O}: 10 denoted with *), irradiation time of 1.5 h, Havar foil thickness of 0.2 mm

process removes only ca. 2.5–4 mg from the disc material. Table 1 lists the target masses before and after the subsequent three bombardments as well as the corresponding mass losses for the irradiated discs 1 and 2.

According to our observation, the method allows to get more than 75% of the total activity, while the rest goes to the WASTE vial or stays on the irradiated disc or the filters. The activity results for the product and the waste vials are presented in Table 2. A dry distillation process removes the target heterogeneities appearing after the subsequent irradiations. In this process, the target material is heated to melt (at 733^{o}C), whereby the surface becomes smooth, and the target can be irradiated again.

Quality control

The last step of production is quality control (QC). First, the sterility test was performed to ensure microbiological purity. Then, after the sample ceased to radiate (about a month after a dry distillation), 0.1 ml of the product was injected into a sterile and fertile tryptic soy broth. Finally, the bottle with the broth and the sample were kept at 25^{o}C for four days and afterwards for another five days in 33^{o}C.

The gamma-ray spectroscopy was employed to acquire the radiation spectrum. The RAYTEST MUCHA multichannel analyzer with the NaI 3x3" detector was used. The 511 keV lines corresponding to the positron-electron annihilation photons and other gamma peaks from the decay were confirmed in the spectra, thus proving the suitability of sodium iodide for diagnostic use.

Finally, the radionuclide purity was tested using a Canberra-Packard gamma spectrometer equipped with high-purity germanium (HPGe) detector. The spectrum of the final product sample (of 0.5 ml volume, the spectral acquisition time of 60 minutes) was obtained two weeks after the synthesis to ensure the degradation of all radioisotopes with shorter half-lives. The spectrum was analyzed using Genie 2000 software, and the radionuclide content was determined to be below 0.1%.

Similarly to other drugs for intravenous injection and according to European Pharmacopoeia [31] all radiopharmaceuticals must be formulated at and maintain an appropriate pH in order to ensure their stability, integrity and safety in medical applications. It is acceptable for the pH of the medically used radiopharmaceuticals to vary between 2 and 9 due to the blood's high buffer capacity, and usually, the pH values of most radiopharmaceuticals are within a range of 4 to 8 [32]. In case of the radioiodine solutions, pH should be maintained at an alkaline level to avoid volatilization of iodine [33, 34]. In our experiment no pH determinations have been performed yet, because it is currently in the optimization phase of the radioisotope production conditions.

Monte Carlo simulations

The main goals of the Geant4 simulations (Fig. 1) involved:

- optimization of the target geometry and the employed materials (as the target and the degradation foils) by selecting their types and thicknesses,
- calculation of the depth of proton penetration,
- optimization of the parameters of the ^{124}I production process,
- characterization of the activities of ^{124}I and other radioisotopes produced during the bombardment.

Simulation: optimization of the target and degradation foil materials and their thicknesses

The influence of the target material type (the natural vs enriched TeO_2) and the applied degrading foil (Havar, Molybdenum or Aluminum) on the ^{124}I production efficiency was analyzed. The physicochemical parameters of the simulated foil materials are collected in Table 3.

In the Monte Carlo simulations, the conditions (like the target size and the type of foil material) were changing, based on the model proposed by Poignant et al. [25] to adapt the process to IBA 18/9 Cyclotron. The foils 0.05–0.5 mm thick and the targets 0.1–1 mm thick were simulated. The target thicknesses and the corresponding masses for the experimental

Table 3 The energy degrading foils characteristics for Aluminum, Molybdenum and Havar

Property	Aluminum	Molybdenum	Havar
Thermal conductivity (W m^{-1} K^{-1})	167	138	13
Melting point (°C)	582	2620	1480
Density (g cm^{-3})	2.7	10.2	8.3

target geometry and the material density are presented in Table 4. The simulation results were compared for two proton beam currents: 10 and 15 μA.

Simulation: depth of proton penetration

SRIM/TRIM 2013 and Geant4 10.04 were used to track 14.8 MeV protons inside the bombarded target and to optimize its amount. The modelling involved more than 100 Monte Carlo simulations for 1000 iterations. Then, the stopping power and the range of incident particles in the target matter and the physical thickness of the target block were estimated. In SRIM/TRIM 2013 a simple geometry was modelled (Fig. 4a), whereas in Geant4 a complex 3D environment was created (Fig. 4b). The penetrations of protons through the target were calculated in both environments and compared. The Bethe's formula to calculate the stopping power as a function of the proton energy E given by equation 1:

$$-\frac{\mathrm{d}E}{\mathrm{d}x} = \frac{4\pi n k_0^2 z^2 e^4}{mc^2\beta^2}[ln\frac{2mc^2\beta^2}{I(1-\beta^2)} - \beta^2] \quad (1)$$

was used to fit the SRIM stopping power values. Its parameters are as follows: $k_0 = 8.99$ x 10^9 Nm^2C^{-2}, (the Coulomb constant), z—atomic number of the heavy particle, e—magnitude of the electron charge, n—number of electrons per unit volume in the medium, m—electron rest mass, c—speed of light in vacuum, $\beta = V/c$—speed of the particle relative to c, I - mean excitation energy of the medium [35].

The ranges R of protons traveling through a medium can be calculated with the inverse of the stopping power using the formula 2:

$$R(E_0) = \int_0^{E_0} \frac{\mathrm{d}x}{\mathrm{d}E}\mathrm{d}E, \quad (2)$$

where the integration is over the proton energy from E_0, which is the energy at which the proton enters the medium, to the point where the proton has lost its energy.

Simulation: ^{124}I production process

Finally, more than 100 simulations and 1000 iterations were performed in the Geant4 toolkit to simulate the ^{124}I production. One thousand iterations allow for ca. 1,000,000 primaries in 15 μA and 625,000 primaries in 10 μA. The simulations were done for the TeO_2 target containing natural Te and for that enriched in ^{124}Te. The simulated model was created based on the GE PETtrace target system adapted to the COSTIS system of IBA 18/9 Cyclotron. The length of the target system and the target dimensions were changed. The quality of the optimized ^{124}I production parameters were checked in the experiment performed for a natural tellurium dioxide target bombarded for 1.5 h with 14.8 MeV protons and beam currents of 10 μA and 15 μA.

Table 4 The target thicknesses and the corresponding TeO_2 masses

Thickness [mm]	**1.0**	**0.8**	**0.5**	**0.3**	**0.1**
Target mass [mg]	640.9	512.7	320.5	192.3	64.1

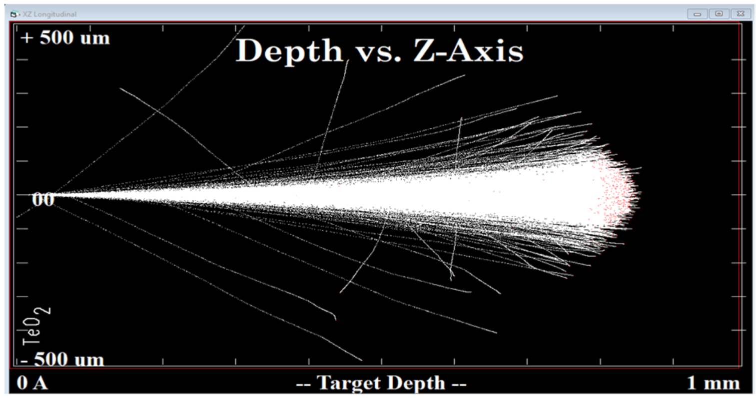

(a) SRIM simulation, 14.8 MeV (18 MeV after interacting with 0.2 mm Havar degradation foil) proton beam interacting with TeO_2 target

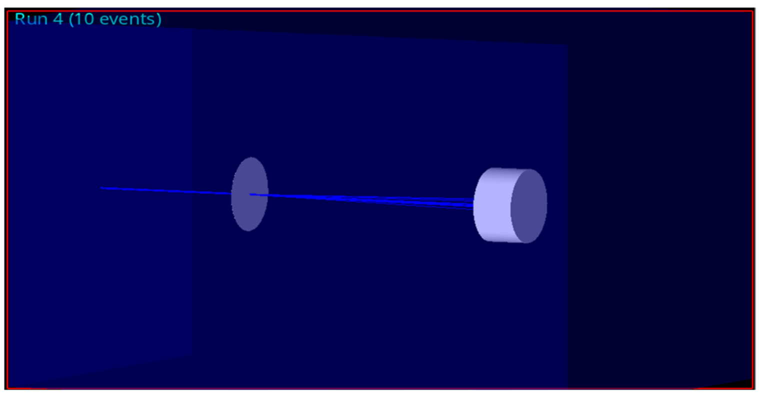

(b) Geant4 simulation, 18 MeV proton beam interacting with 0.2 mm Havar foil and next with TeO_2 target (example with 10 events)

Fig. 4 Simulated IBA 18/9 cyclotron geometries. **a** A simple SRIM/TRIM model and **b** a complex geometry of the cyclotron irradiation system created in GEANT4

Experiment

The TeO_2 irradiation was repeated nine times using 10 μA proton beam and 34 kV RF during 1.5 h and performed only once for 15 μA proton beam and the same other parameters (unfortunately, a higher activation resulted in the cyclotron target radiation damage). The finished product was evaluated and tested through various quality checks. All activity measurements were carried out using the NUVIA ISOMED Dose Calibrator.

PET-CT verification

The PET/CT acquisition was performed using a Biograph mCT PET/CT system manufactured by Siemens Healthcare (Erlangen, Germany) to visualize the $\beta+$ radioisotopes, like ^{123}I and ^{124}I. The PET/CT protocol included a standard 18F-FDG scan. A cylindrical Jaszczak phantom (Data Spectrum Corporation, Durham, NC, USA) (diameter of 21.6 cm and a volume of 6.9 L) with the micro-spheres (of the 9.5, 12.7, 15.9, 19.1, 25.4, and 31.8 mm diameters) was used for the test purposes. An iterative True-X reconstruction + TOF (the algorithm proposed by Siemens and based on the Point Spread Function (PSF) method with an additional correction) was applied. The settings of the reconstruction algorithm were as follows: 2 iterations and 21 subsets, a Gaussian filter of 3 mm, a 256 × 256 × 75 matrix (voxel spacing 3.1819 × 3.1819 × 3.00 mm) with a Time Of Flight correction. Additionally, the following ^{124}I acquisition parameters presented elsewhere were also used for a sake of comparison:

- OSEM 4 iterations, 16 subsets, Gaussian filter 5 mm [36];
- OSEM 2 iterations, 16 subsets, Gaussian filter 6.4 mm [37];
- OP-OSEM 3 iterations, 21 subsets, Gaussian filter 5 mm [38];
- OSEM-TOF+PSF 2 iterations, 21 subsets, Gaussian filter 3 mm [39].

The settings from this study, similar to those in [39], are routinely used in the medical PET examinations at our hospital.

Results

Optimization of the material and the degradation foil type and thickness

As reveals from Figs. 5, 6 and 7, when the target material fills the cavity of a platinum disc (the target thickness of 1 mm), the ^{124}I production from natural Te requires the energies close to 18 MeV. When the target thickness is < 0.5 mm, the maximum yield is obtained for the energies around 13 MeV, which corresponds to the maximum cross section for ^{124}Te(p,n)^{124}I reaction—such energies can be obtained using the degrading foil 0.2–0.3 mm thick.

In the case of the ^{124}Te enriched targets, similar trends are seen, namely the energy of 17-18 MeV is optimal for the thick target (1 mm), whereas for a thinner one (< 0.5mm) the optimum shifts to 13 MeV, like in case of natural Tellurium dioxide, however, the activity values are almost an order of magnitude higher.

At 14.8 MeV, independently of the target type and the beam current used, the amount of the produced ^{124}I increases with the target thickness up to 0.5 mm, then the trend becomes reversed.

The beam current is another significant parameter affecting the ^{124}I yield, as expected (Figs. 5, 6, 7). With higher current the yield should be higher, because more particles can interact with the target. As revealed from the simulations, the target thickness plays a crucial role in the ^{124}I production at the energy of 14.8 MeV. For the 0.5 mm target, the maximum activity of the obtained iodine is approximately 185 MBq after 1.5 h irradiation with the proton beam of 10 μA, and 259 MBq for 15 μA. The activities up 370 MBq for 15 μA and the enriched target can be obtained for the thicker targets.

The densities of the foil materials are as follows: Molybdenum > Havar > Aluminum (Table 3). The abilities of the individual foils to slow down the proton energy with the thinnest foil layer fulfil the same relationship. In the case of the natural TeO_2 the best results could be obtained with Aluminum foil, but only the activities of up to 74 MBq at the end of the irradiation were available (Fig. 7).

Experimental versus simulated ^{124}I activities

The test with soy broth showed no turbidity, which indicates the ^{124}I NaI sample sterility. The multi-channel analyser (RAYTEST MUCHA) showed the 511 keV peaks from the annihilation processes, and the gamma spectrum revealed the peaks at 603

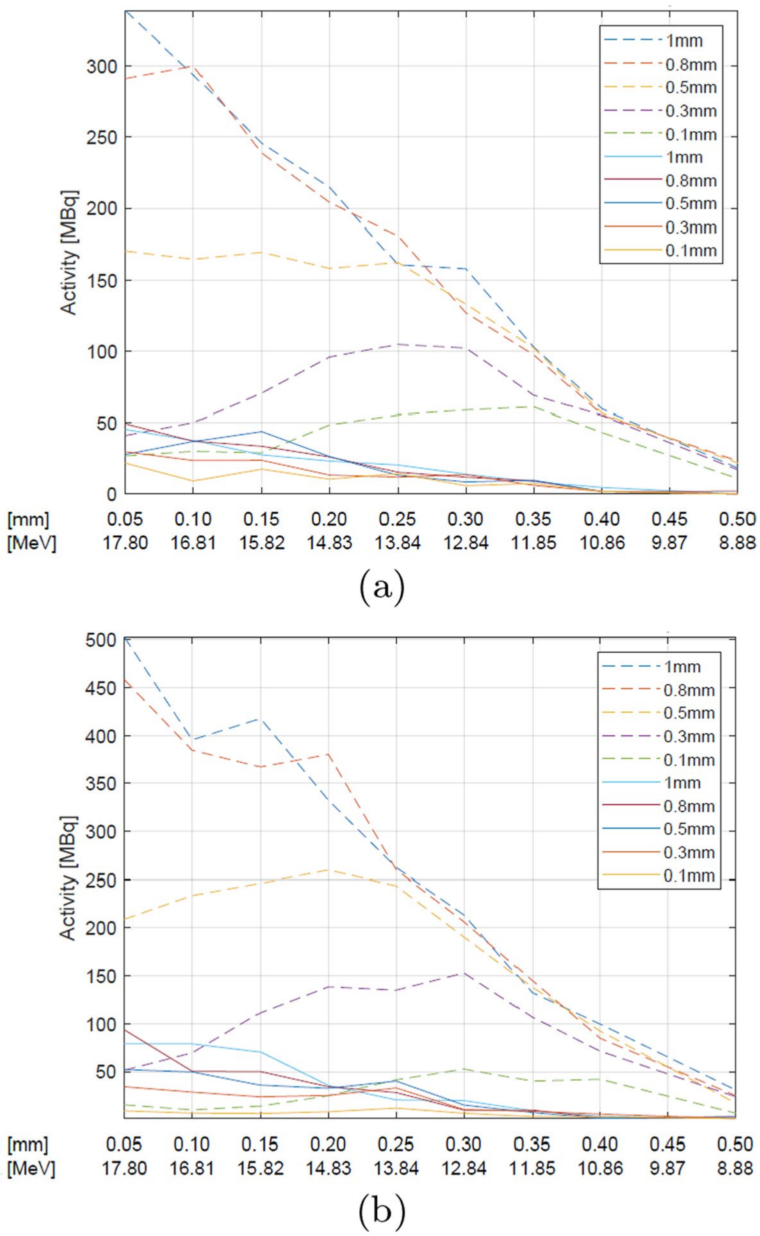

Fig. 5 The simulated activity changes of ^{124}I from natural (straight line) and enriched (dashed line) TeO_2 for various target thicknesses (denoted by various colors as shown in the legend) and various Havar foil thicknesses at the proton current of **a** 10 μA and **b** 15 μA

keV and 1690 keV from the ^{124}I decay as well as the peaks from the ^{123}I decay (158 keV) and the annihilation process (511 keV) (Fig. 8).

Table 5 presents the total activities after the irradiation and separation as well as the corresponding estimated values.

The Monte Carlo simulated values were calculated for the irradiation-separation times equal exactly to the experimental values. The experimental activities at the end of separation (EOS) were compared with the activities from the Monte Carlo simulations.

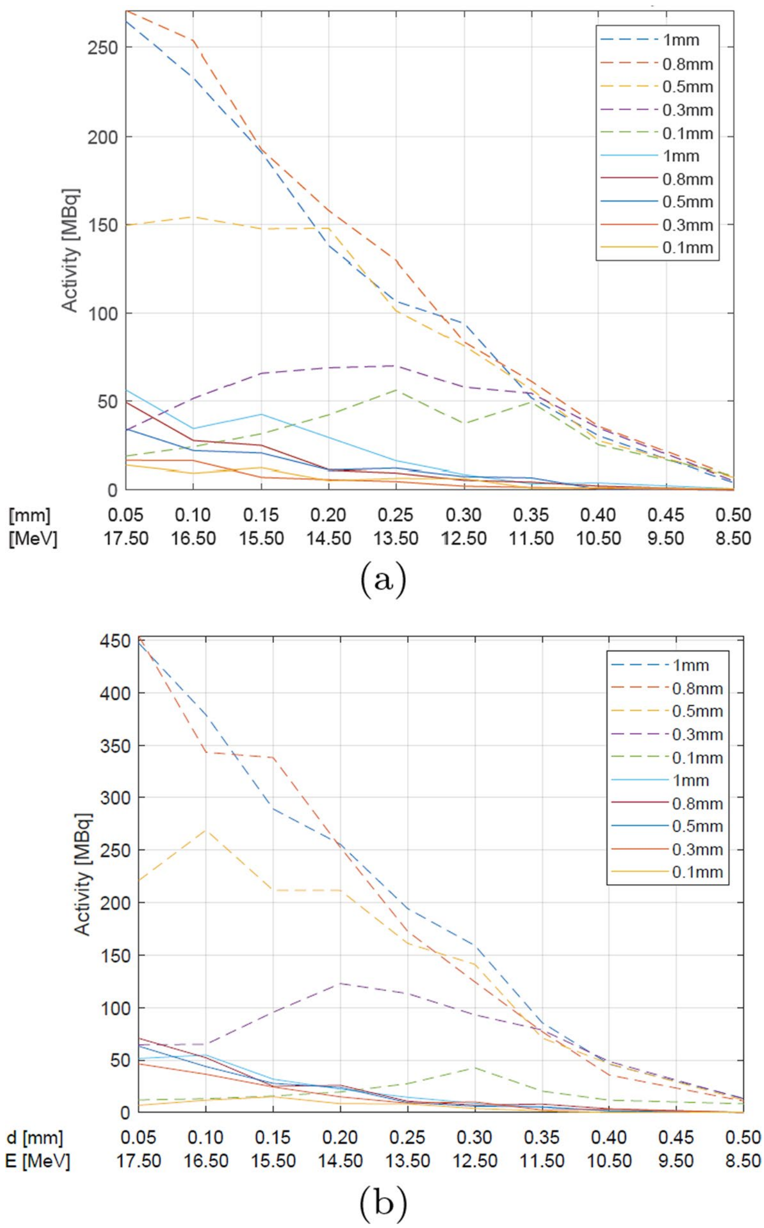

Fig. 6 The simulated activity changes of ^{124}I from natural (straight line) and enriched (dashed line) TeO_2 for various various target thicknesses (denoted by various colors as shown in the legend) and various Molybdenum foil thickness at the proton current of **a** 10 µA and **b** 15 µA

For the natural $^{124}TeO_2$ target the maximum estimated ^{124}I activity is 34.41 MBq for irradiation parameters: 14.8 MeV, 10 µA, Havar 0.2 mm and 50.32 MBq for parameters: 14.8 MeV, 15 µA, Havar 0.2 mm. The corresponding experimental values are 25.16 and 56.61 MBq, respectively for 10 µA and 15 µA (Table 5).

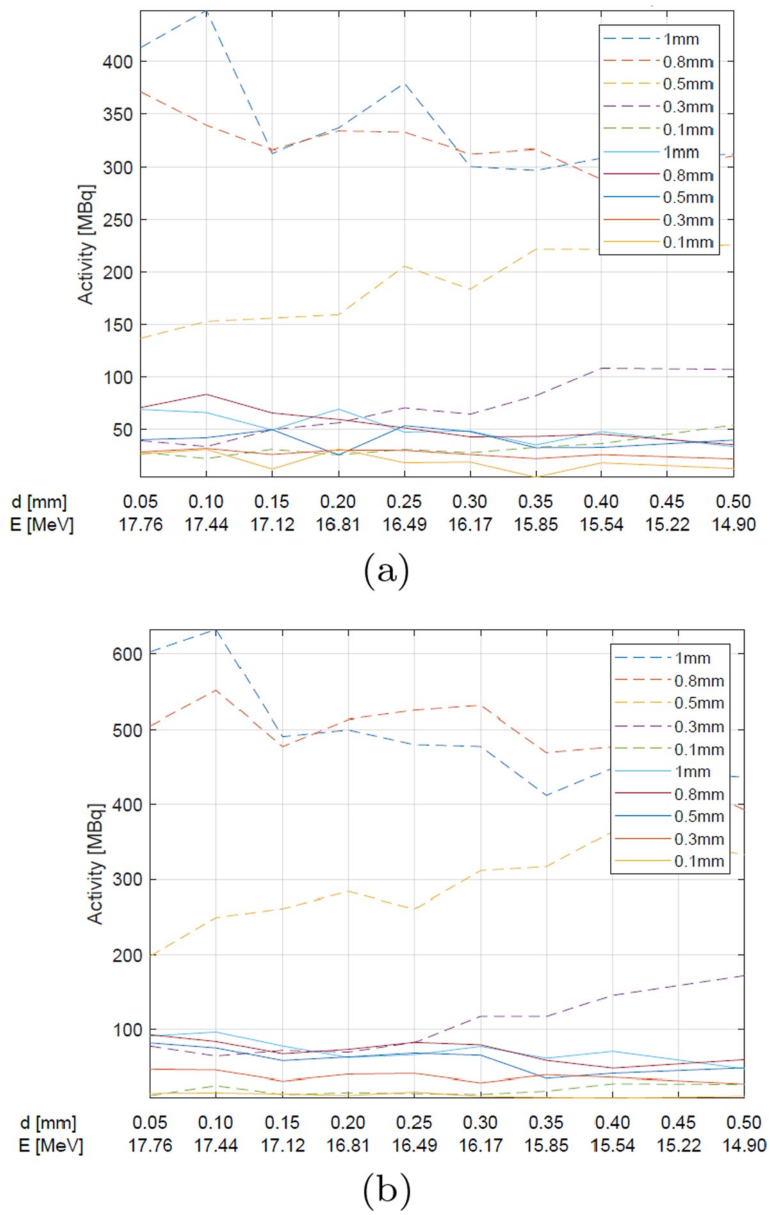

Fig. 7 The simulated activity changes of ^{124}I from natural (straight line) and enriched (dashed line) TeO_2 for various target thickness (denoted by various colors as shown in the legend) and various Aluminum foil thickness at the proton current of **a** 10 µA and **b** 15 µA

Simulation: depth of proton penetration

14.8 MeV proton penetration ranges numerically calculated for the TeO_2 target are similar in both, Geant4 and SRIM/TRIM methods and equal 812.8 ± 15.1 µm and 866.0 ± 23.7 µm, respectively.

The proton range depends on the capture cross-section and the material the protons interact with as they are slowed down. The energy of the bombarding beam varies with depth of penetration and the cross-section for the nuclear reaction of interest varies with bombarding energy. A large part of the protons' energy is distributed at the end

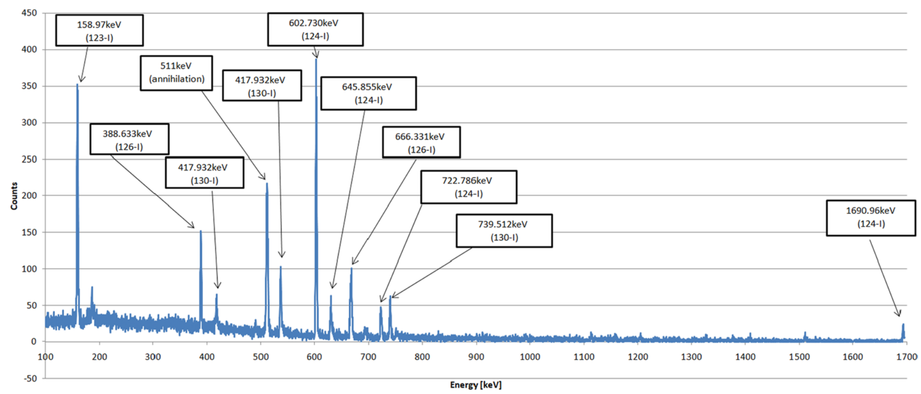

Fig. 8 HPGe spectrum.The peaks from the ^{124}I decay: at 603 keV, 645 keV, 722 keV and 1690 keV, and from the ^{123}I decay (158 keV), and also ^{126}I (388 keV and 666 keV) and ^{130}I (417 keV and 739 keV) as well as the annihilation process (511 keV) are indicated

Table 5 The activities obtained in the natural TeO_2 irradiations

N^{O}	Time [h]	Activity EOS [MBq]	Simulated activity EOS [MBq]	Difference: experiment versus simulation [%]
1	73.88	20.72	33.30	60.71
2	118.14	13.69	24.79	81.08
3	122.77	14.43	24.42	69.23
4	96.50	18.50	28.12	52.00
5	131.36	15.91	23.68	48.83
6	72.39	20.72	34.04	64.28
7	70.44	25.16	34.41	36.76
8	70.89	23.31	34.41	47.62
9	144.87	14.43	22.20	53.85
10*	71.49	56.61	50.32	11.11

The irradiation parameters: the proton beams of 10 μA (N^{O}: 1-9) and of 15 μA (N^{O}: 10 denoted with *), irradiation time of 1.5 h, the thickness of the Havar foil: 0.2 mm. The results are obtained at the end of separation (EOS) and Time [h] is the time difference between the end of bombardment and the end of separation

of their trajectories forming the Bragg peak, and the amount of charge determines its shape—a higher charge results in a narrower peak. As reveals from Fig. 9 and the SRIM calculations the targets of the thicknesses >0.8 mm significantly reduce the energy of the bombarding particles or completely absorb the beam; thus, such targets can be considered as thick.

Figures 9 and 10 shows the exemplary proton ranges distribution in the TeO_2 target obtained using SRIM/TRIM 2013 and Geant4.

Simulation: ^{124}I production process

The production of ^{124}I was predicted through modelling of the ^{124}Te(p,n) reaction at the proton energy of 14.8 MeV, taking into account also the (p,xn) reactions when analyzing the contamination products. The simulated activities of ^{124}I as well as of the impurities, like ^{123}I,^{125}I,^{126}I and ^{130}I were calculated and the results are shown in Tables 6, 7, 8 and 9.

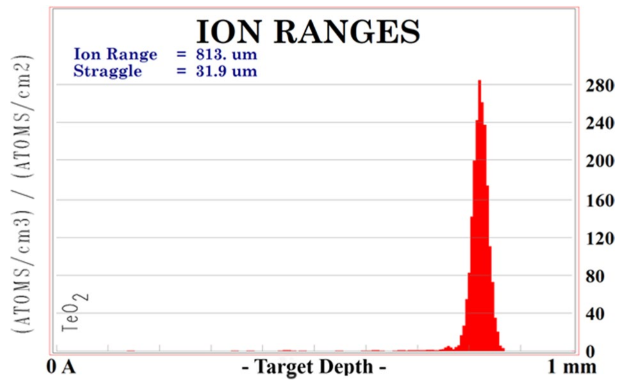

Fig. 9 SRIM/TRIM experiment. An exemplary stopping range for protons (14.8 MeV) in Tellurium dioxide target. The peak of distribution is for 813.0 μm

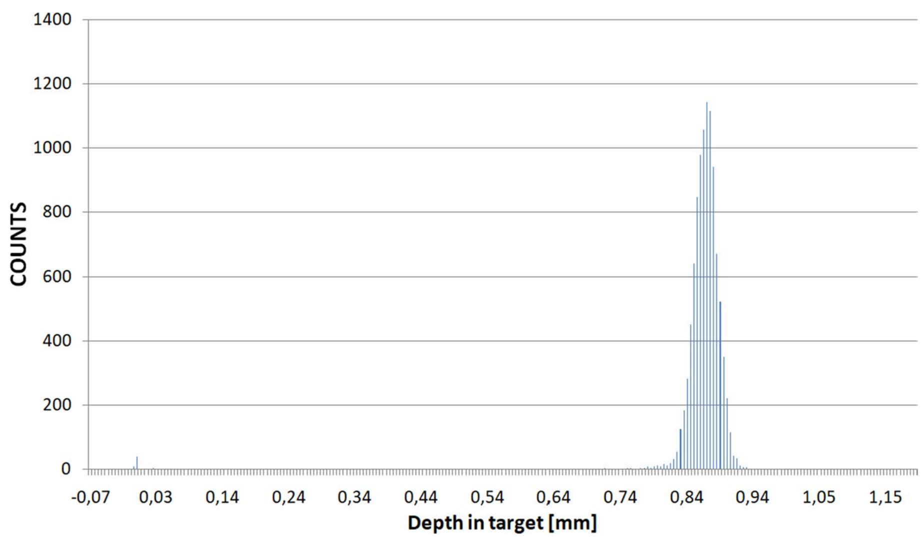

Fig. 10 Geant4 experiment. An exemplary stopping range for protons (14.8 MeV) in Tellurium dioxide target. The peak of distribution is for 886.2 μm

As expected, when using natural tellurium dioxide, the theoretical activity of the produced ^{124}I radioisotope is almost one order of magnitude smaller (23.199 MBq and 35.594 MBq for 10 μA and 15 μA, respectively) than in case of the Te enriched target (214.785 MBq and 332.334 MBq for 10 μA and 15 μA, respectively), whereas the amount of the produced impurities is much higher—60% vs 12% of the total yield (Tables 7, 8). The calculated total activities after 72 h since the bombardment are 34.003 MBq and 50.135 MBq for the proton currents of 10 μA and 15 μA, respectively (Tables 8, 9), whereas the corresponding experimental activities after 72 h are ca. 25.16 MBq and 56.61 MBq (Table 5); however, the latter value is from a single experiment.

Measurement: ^{124}I verification via PET-CT

Finally, we performed the PET-CT study to capture the radioactivity emanating from ^{124}I. Two tests were done: in the first test one sphere (diameter = 19.1 mm) was

Table 6 The results of the Monte Carlo simulation of the ^{124}I production process

Radioisotope	Half Life	Decay mode	EOB [MBq]	EOB [%]	After 72 h [MBq]	After 72 h [%]
^{6}He	806.7 ms	β-	72.483	1.24	0	0
^{119}I	19.1 min	EC $\beta+$	138.010	2.36	0	0
^{120}I	81.6 min	EC $\beta+$	76.664	1.31	0	0
^{122}I	3.6 min	EC $\beta+$	717.393	12.27	0	0
^{123}I	13.2 h	EC $\beta+$	672.623	11.51	15.429	10.38
^{124}I	**4.2 d**	**EC $\beta+$**	**214.711**	**3.67**	**130.499**	**87.71**
^{13}N	9.9 min	EC $\beta+$	3794.831	64.92	0	0
^{14}O	70.6 s	EC $\beta+$	143.449	2.45	0	0
^{119}Sb	38.2 h	EC	3.848	0.07	1.036	0.70
^{122}Sb	2.7 d	β- (97.59%), EC $\beta+$ (2.41%)	1.147	0.02	0.518	0.35
^{119}Te	16.1 h	EC $\beta+$	8.991	0.15	0.407	0.27
^{121}Te	19.2 d	EC $\beta+$	0.962	0.02	0.888	0.59
Total			5845.112	100.00	148.777	100.00

The production parameters: TeO_2 **enriched** in ^{124}Te, 18 MeV protons moderated to 14.8 MeV with 0.2 mm Havar, the proton current of 10 μA. The activity values at the end of bombardment (EOB) and the activity values after 72 hours since the end of bombardment are presented. ^{124}I is highlighted in bold

Table 7 The results of the Monte Carlo simulation of the ^{124}I production process

Radioisotope	Half Life	Decay mode	EOB [MBq]	EOB [%]	After 72 h [MBq]	After 72 h [%]
^{118}I	13.7 min	EC $\beta+$	71.447	0.85	0	0
^{119}I	19.1 min	EC $\beta+$	69.449	0.83	0	0
^{120}I	81.6 min	EC $\beta+$	77.182	0.92	0	0
^{121}I	2.12 h	EC $\beta+$	223.904	2.67	0	0
^{122}I	3.6 min	EC $\beta+$	1732.821	20.69	0	0
^{123}I	13.2 h	EC $\beta+$	1151.958	13.75	26.455	11.46
^{124}I	**4.2 d**	**EC β+**	**332.334**	**3.97**	**201.983**	**87.50**
^{13}N	9.9 min	EC $\beta+$	4972.319	59.36	0	0
^{118}Sb	3.6 min	EC $\beta+$	72.187	0.86	0	0
^{119}Sb	38.2 h	EC	1.924	0.02	0.518	0.23
^{118}Te	6.0 d	EC	0.518	0.01	0.370	0.16
^{119}Te	16.1 h	EC $\beta+$	4.514	0.05	0.185	0.09
^{121}Te	19.2 d	EC $\beta+$	1.480	0.02	1.332	0.57
Total			8712.02	100.00	230.843	100.00

The production parameters: TeO_2 **enriched** in ^{124}Te, 18 MeV protons moderated to 14.8 MeV with 0.2 mm Havar, the proton current of 15 μA. The activity values at the end of bombardment (EOB) and the activity values after 72 hours since the end of bombardment are presented. ^{124}I is highlighted in bold

filled with the final product from the natural TeO_2 irradiation (Fig. 11a), whereas the remaining spheres contained distilled water.

In the second test, the smaller sphere (diameter = 15.9 mm) was filled with the distilled ^{124}I, whereas the larger one (diameter = 19.1 mm) with ^{18}F, and the remaining ones contained distilled water (Fig. 11b). As seen in Fig. 11a, b $\beta+$ emitter positrons are present in both cases, confirming the applicability of both products in PET/CT imaging.

Table 8 The results of the Monte Carlo simulation of the ^{124}I production process

Radioisotope	HalfLife	Decay mode	EOB [MBq]	EOB[%]	After72h[MBq]	After72h[%]
^{11}Be	13.8 s	β-	72.483	0.87	0	0
^{6}He	806.7 ms	β-	72.483	0.87	0	0
^{120}I	81.6 min	EC $\beta+$	38.739	0.46	0	0
^{122}I	3.6 min	EC $\beta+$	434.972	5.19	0	0
^{123}I	13.2 h	EC $\beta+$	65.786	0.79	1.517	4.44
^{124}I	**4.2 d**	**EC β+**	**23.199**	**0.28**	**14.097**	**41.47**
^{125}I	59.4 d	EC	3.552	0.04	3.404	10.06
^{126}I	12.9 d	EC $\beta+$ (52.7%), β- (47.3%)	14.319	0.17	12.173	35.84
^{128}I	24.9 min	β- (93.1%), EC $\beta+$ (6.9%)	3326.115	39.71	0	0
^{130}I	12.4 h	β-	157.916	1.89	2.775	8.19
^{13}N	9.9 min	EC $\beta+$	3979.609	47.51	0	0
^{14}O	70.6 s	EC $\beta+$	72.483	0.87	0	0
^{15}O	122.2 s	EC $\beta+$	72.483	0.87	0	0
^{129}Te	69.6 min	β-	42.92	0.51	0	0
Total			8377.059	100.00	33.966	100.00

The production parameters: **natural** TeO_2, 18 MeV protons moderated to 14.8 MeV with 0.2 mm Havar, the proton current of 10 μA. The activity values at the end of bombardment (EOB) and the activity values after 72 hours since the end of bombardment are presented. ^{124}I is highlighted in bold

Table 9 The results of the Monte Carlo simulation of the ^{124}I production process

Radioisotope	Half Life	Decay mode	EOB [MBq]	EOB [%]	After 72 h [MBq]	After 72 h [%]
^{6}He	806.7 ms	β-	71.817	0.86	0	0
^{119}I	19.1 min	EC $\beta+$	69.079	0.82	0	0
^{120}I	81.6 min	EC $\beta+$	38.406	0.46	0	0
^{121}I	2.12 h	EC $\beta+$	111.370	1.33	0	0
^{122}I	3.6 min	EC $\beta+$	1221.111	14.58	0	0
^{123}I	13.2 h	EC $\beta+$	70.596	0.84	1.628	3.23
^{124}I	**4.2 d**	**EC β+**	**35.594**	**0.42**	**21.608**	**43.13**
^{125}I	59.4 d	EC	3.996	0.05	3.848	7.66
^{126}I	12.9 d	EC $\beta+$ (52.7%), β- (47.3%)	17.316	0.21	14.726	29.38
^{128}I	24.9 min	β- (93.1%), EC $\beta+$ (6.9%)	5404.738	64.52	0	0
^{130}I	12.4 h	β-	361.527	4.32	6.364	12.72
^{13}N	9.9 min	EC $\beta+$	5161.833	61.62	0	0
^{14}O	70.6 s	EC $\beta+$	143.671	1.71	0	0
^{119}Sb	38.2 h	EC	1.928	0.02	0.518	1.04
^{122}Sb	2.7 d	β- (97.59%), EC $\beta+$ (2.41%)	1.147	0.01	0.518	1.05
^{119}Te	16.1 h	EC $\beta+$	4.514	0.05	0.185	0.40
^{121}Te	19.2 d	EC $\beta+$	0.666	0.01	0.592	1.16
^{127}Te	9.4 h	β-	22.681	0.27	0.111	0.22
^{129}Te	66.6 min	β-	42.513	0.51	0	0
Total			12784.503	100.00	50.098	100.00

The production parameters: **natural** TeO_2, 18 MeV protons moderated to 14.8 MeV with 0.2 mm Havar, the proton current of 15 μA. The activity values at the end of bombardment (EOB) and the activity values after 72 hours since the end of bombardment are presented. ^{124}I is highlighted in bold

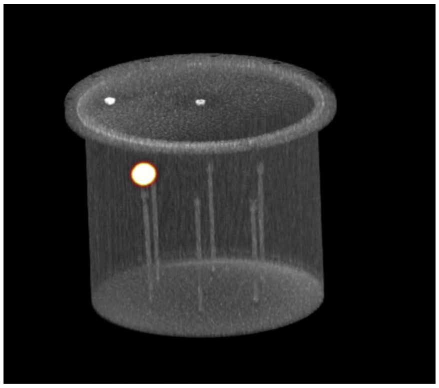

(a) Phantom with ^{124}I

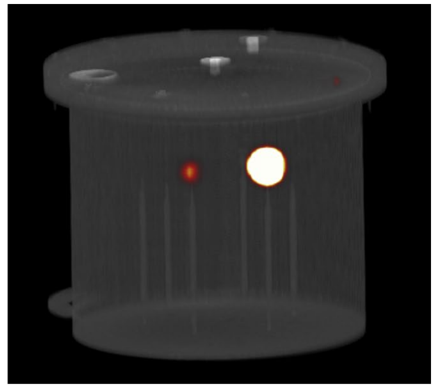

(b) Phantom with ^{18}F and ^{124}I

Fig. 11 PET/CT phantom acquisition using a cylindrical Jaszczak Phantom (Data Spectrum Corporation, Durham, NC, USA), the diameter of 21.6 cm and a volume of 6.9 L, with the microspheres (9.5, 12.7, 15.9, 19.1, 25.4, and 31.8 mm diameter)

Discussion

The ^{124}I has been extensively investigated for the last several years. Although ^{124}I is now well-known [40–44], its efficient extraction is still a problem, which limits its use in diagnostics and research. Also, Iodine-124 production data is vast—many alternative nuclear production pathways exist, encompassing a wide range of reactions [45, 46].

However, the clinical applications of this radioisotope are limited owing to its very high production cost and lack of widespread availability [47]. The interest in ^{124}I applications is expected to grow, as it can be attached to the cell surface and used in cell labelling, opening new possibilities in the studies of human metabolism [4, 48]. Only about 23% of its disintegration is *via* positron emission of relatively high energy [6]. The other decay processes involve emissions of high-energy γ rays, some in cascade with the positrons [7]. Gamma radiation increases the radiation dose in the patients and complicates the dose calculations; however, the $\beta+$ presence makes this radioisotope suitable for PET studies [35]. On the other hand, Auger electron emission (electron yield per decay = 8.6, [49]) gives it the capability to be named a theranostic agent [50–52]. However, a theranostic approach on Iodine-124 is not yet proved and consolidated [53]. ^{124}I finds, however, its application, collectively with ^{131}I, as a part of a theranostic pair [54]. Such pairs, formed of the similar and matching radionuclides, better serve diagnostic purposes by lowering radiation burden and achieving better image quality [55].

In our work the ^{124}Te(p,xn) reactions, the most effective in the natural TeO_2+Al_2O_3 target and in the target enriched with ^{124}Te irradiated with 14.8 MeV protons, were simulated in the Monte Carlo code. The results of the simulations were compared with the experimental data obtained for the natural TeO_2+Al_2O_3 target. The degradation Havar foil, optimized *via* simulations to be 0.2 mm thick, was also applied in the experiment.

As revealed from the SRIM/TRIM and Geant4 simulations, for the natural $^{124}TeO_2$ targets irradiated with 14.8 MeV proton beams, the thicknesses >0.8 mm are required to markedly reduce the energy of the bombarding particles or to completely absorb the bombarding beam. A too thin layer would make protons fly through it without ^{124}I production, whereas a too thick one unnecessarily increases the costs of the production, especially in the case of tellurium enriched $^{124}TeO_2$, and the risk of the target overheating [56]. Moreover, because the dry distillation is used to separate ^{124}I from the disk, the thickness of the material cannot be too great. In natural TeO_2 ^{124}I has a maximum cross-section at >14 MeV—so is produced very close to the surface of the target and diffuses out faster compared to ^{130}I, which has its maximum cross-section at much lower energy and is, thus, produced deeper in the target [57]. Therefore, the distillation parameters should be optimized individually, which is especially important when optimizing the production from natural tellurium. As shown by Scholten et al. [19], at the incident energy of 14.8 MeV the ^{123}I production from the reaction $^{124}Te(p,2n)^{123}I$, concurrent to $^{124}Te(p,n)^{124}I$, is slightly higher than of ^{124}I [19]. The amount of the co-produced iodine ^{123}I is high, but 48 h since irradiation its activity decreases below 10% of the initial value, whereas that of ^{124}I drops to ca. 75%. It is due to the large difference in the half-lives of both radionuclides (Table 6).

Of interest are also the reactions (p,2n) and (p,3n) on the long-lived ^{125}I ($T_{1/2}$= 60.2 days), ^{125m}Te ($T_{1/2}$= 57.40(15) days) and the stable ^{125}Te and ^{126}Te nuclei. It was established that the content of the ^{125}I and ^{126}I impurities depends on the protons' energy and the thickness of the target material. In the (p,n) reaction, the yield of ^{126}I is somewhat smaller than that in the (d,2n) reaction; the amount of ^{125}I drops markedly below that of ^{126}I, and ^{131}I could not be detected at all [19]. Unfortunately, due to the high natural abundances of other radioisotopes, like ^{125}Te (7.07%) and ^{126}Te (18.84%) in natural tellurium, the reactions like (p,2n) and (p,3n) may become of importance by increasing the amount of the radiochemical radioiodine contaminants and affecting the final yield of iodine ^{124}I.

At the end of the final product separation (it contains ^{124}I and the radioactive impurities), the experimental activities were 25.16 MBq and up to 56.61 MBq for 14.8 MeV protons at 10 μA and 15 μA, respectively. The Monte Carlo simulations of the reactions $^{124}Te(p,xn)$ used to estimate the amount of the produced radioisotope based on the disk geometry and the cyclotron operating parameters yielded up to 34.003 MBq (10 μA) for the natural target, and 50.135 MBq (15 μA) for the Te enriched target. Thus, for the natural TeO_2 there are some relative discrepancies between the simulated values and the experimental data—for the beam current of 10 μA the simulated activity is about 30% higher than the measured one, whereas, in the case of 15 μA proton beam, it is ca. 12% lower. They are presumably due to the differences in the simulated and experimental target volumes. In the simulations, the target material was assumed to fill the whole cavity, whereas in the experiments, the target material, after melting, filled up slightly less than the entire volume intended for it. Moreover, the applied proton current and the successive re-irradiations are of importance: the production yields can be enhanced by increasing the proton beam current, but the maximum beam deposited on a target is limited by the targetry, including the thermal characteristics of the target material and the cooling system to prevent a possible loss of the target material due to inhomogeneous distribution of temperature resulting in appearance of a subsequent local target burnt-up areas [58]. They disappear, however, after the dry-distillation processes. Thus, once prepared, the target can be used many times until its thickness is significantly reduced. In the experiment, the loading of about 400 mg of tellurium dioxide with aluminium oxide was applied, and the mass losses after the subsequent dry distillations were of about 2.5-4 mg. Thus, to obtain a close agreement between the simulated and experimental values, these processes should be taken into account. The experimental yield is also influenced by a beam profile and an intensity, the radiation damage effects and a chemical separation yield [57, 59]. In the case of the proton beam of 15 μA, an additional source of error is the lack of repeated measurements (due to the target disruption). Thus, the obtained activity value is presumably overestimated. Also, more repetitions would undoubtedly improve the statistical strength for the beam of 10 μA (9 re-irradiations). Furthermore, because tellurium is the radioisotopes mixture in its natural form, the radioactive pollution level is very high, as many, mainly short-lived, radioisotopes can be produced on irradiation by the (p xn) reactions and the reactions with neutrons. For instance, after the end of the bombardment the most abundant ones, like ^{13}N ($T_{1/2}$=9.97 min),^{128}I ($T_{1/2}$=24.99 min), ^{122}I ($T_{1/2}$=3.63 min), ^{123}I ($T_{1/2}$=13.2 h) and ^{130}I ($T_{1/2}$=12.36 h), decay fast and after 72 h some of them disappear, changing the mutual relative proportions within the product. In effect, the relative ^{124}I levels increase from 0.28% to 41.47% and from 0.96 to 43.13% at 10 μA and 15 μA, respectively (Tables 8, 9), as calculated in the Monte Carlo simulations. For the Te enriched target the corresponding increases are from 3.67% to 87.71% and from 8.98% to 87.50% at 10 μA and 15 μA, respectively (Tables 6 and 7). For the natural target the main impurities come from ^{126}I, ^{125}I and ^{130}I (Tables 8 and 9), whereas for the Te enriched target almost exclusively from ^{123}I (Tables 6 and 7). According to European Pharmacopeia [31] the contribution from ^{123}I should be lower or equal to 0.35% of the total activity. We calculated the time when such activity is reached using Monte Carlo simulations. This value was then used to recalculate the activities of the radioisotopes present in the final product vial. The results obtained for the natural and enriched targets are shown in Table 10. As seen from the comparison, enriched tellurium dioxide is more efficient: the post-reaction impurities are at a much lower level (approx. 2%), whereas the main product of the reaction, ^{124}I, accounts for ca. 98% of the total activity. In the case of natural tellurium dioxide, the impurities are of longer half life times (mainly ^{125}I with $T_{1/2} = 59.4$ d and ^{126}I with $T_{1/2} = 12.9$ d) than ^{124}I ($T_{1/2} = 4.18$ d)—though the final product is more polluted, ^{124}I is separated via its distillation from the tellurium oxide matrix.

The separation process adds, however, to the discrepancy between the theoretical and experimental values of the yields. To separate iodine from the $TeO_2 + Al_2O_3$ target, the sublimation process is employed. This procedure allows more than 75% of the

Table 10 The activities for ^{124}I and the radionuclidic impurities calculated at the moment when the contribution of the radioactive impurities from ^{123}I is less than 0.35% of the total activity

Target	Current [μA]	Time from EOB [h]	^{124}I [MBq]	^{124}I [%]	^{123}I [MBq]	^{123}I [%]	Impurities [MBq]	Impurities [%]
Natural $^{124}TeO_2$	10	127	9.62	40.23	0.74	0.35	10.767(^{126}I), 3.33 (^{125}I)	44.98 (^{126}I), 13.90 (^{125}I)
	15	122	15.318	45.25	0.111	0.35	13.172 (^{126}I), 3.737 (^{125}I)	38.95 (^{126}I), 11.09 (^{125}I)
Enriched $^{124}TeO_2$	10	149	76.627	98.01	0.259	0.35	0.777 (^{14}O), 0.259 (^{123}I)	0.99 (^{14}O), 0.35 (^{123}I)
	15	151	117.327	98.34	0.407	0.35	1.184(^{14}O), 0.407(^{123}I)	0.98 (^{14}O), 0.35 (^{123}I)

radioactive substance to be extracted from the target material. The distillation efficiency depends on the temperature, the flow rate of the transporting gas, and the operating time. When the radioisotope loss during the separation is included in the calculations, the experimental values are closer to the simulated ones, at least for the proton beam of 10 μA. Our yield results were compared with the literature data and presented in Table 11.

This comparison also favours enriched tellurium dioxide in ^{124}I production. However, the natural tellurium dioxide costs ca. 20$ per gram, whereas the tellurium dioxide enriched in ^{124}Te costs ca. 10000$ per gram. In view of such huge difference in the targets' costs, even the lower activities of ^{124}I from the natural Te are not deterrent, the more that they are suitable for PET applications, as the obtained radioactive solution contains β^+ radioactive isotope. Taking into account the pros and cons of the natural Te vs. enriched Te targets and the range of the possible applications of ^{124}I it may be stated that the production methodology of this radionuclide from the natural Te material is worth to be further developed. Even if it gives lower yields, the decision to explore such a route opens the possibility to widen the clinical use of ^{124}I and to expand the capability of radioisotope production based on small medical cyclotrons.

Conclusions

The optimization of radioisotope production is a key issue in maximizing the production yield and minimizing the associated costs. An efficient approach to this problem is the use of Monte Carlo simulations prior to the experiment. It allows to make a cost-free optimization of the most influential production factors, determine the final product contamination, and choose the experimental methodology, especially when the expensive Te enriched targets are planned to be applied in the production. However, a semi-empirical adjustment of the ^{124}I production conditions from natural Te is also recommended, especially in view of a vast difference in the targets' costs. The experimental efficiency for such target revealed to be better than 41% with an average thick target (> 0.8 mm) yield of 1.32 MBq/μAh.

Table 11 Comparison of ^{124}I production yield

Reaction	Target	Energy [MeV]	Yield [MBq/μAh]	References
^{124}Te(p,n)^{124}I	**TeO_2**	**15 → 8**	**32.16 (S)**	[60]
^{124}Te(p,n)^{124}I	TeO_2 +Al_2O_3 (5%)	11.6 → 0	6.88 (E)	[61]
^{124}Te(p,n)^{124}I	TeO_2	12.6	13.0 (E)	[62]
^{124}Te(p,n)^{124}I	TeO_2 +Al_2O_3	13 → 9	20 (E)	[19]
^{124}Te(p,n)^{124}I	TeO_2 +Al_2O_3	12.5 → 5	9.0 (E)	[18]
^{nat}Te(p,xn)^{124}I	**TeO_2**	**35 → 22**	**36.63 (S)**	[60]
^{nat}Te(p,xn)^{124}I	**TeO_2**	**10 → 20**	**0.001 (S)**	[63]
^{nat}Te(p,xn)^{124}I	TeO_2	29.5 → 20	3.95 (E)	[60]
^{124}Te(p,n)^{124}I	**TeO_2 + Al_2O_3 (5%)**	**14.8**	**14.5 (S)**	*
^{nat}Te(p,xn)^{124}I	**TeO_2 + Al_2O_3 (5%)**	**14.8**	**1.58 (S)**	*
^{nat}Te(p,xn)^{124}I	TeO_2 + Al_2O_3 (5%)	14.8	1.36 (E)	*

*This work, S, simulation; E, experiment

Thus concluding, Monte Carlo is a powerful tool for studying small medical cyclotron radioisotope production performance. Furthermore, this is a cost-efficient approach to studying new radioisotope production mechanisms before investing in costly experimental studies as well as in the case of long-lasting experiments.

Acknowledgements
Calculations were performed on the Radogost computer cluster at Maria Sklodowska-Curie National Research Institute of Oncology Gliwice Branch and Ziemowit computer cluster at the Laboratory of Bioinformatics and Computational Biology, Biotechnology Center, Silesian University of Technology, both created in the EU Innovative Economy Programme POIG.02.01.00-00-166/08 and expanded in the POIG.02.03.01-00-040/13 project.

Author Contributions
PB: manuscript preparation, methodology selection, dry distillation production process, target preparation, Monte Carlo simulations, DB: manuscript preparation, Monte Carlo simulations, KG: manuscript preparation, methodology selection, dry distillation production process, target preparation, Monte Carlo simulations, AC: manuscript preparation, methodology selection, target irradiation KD: manuscript preparation, reagents supply IG: manuscript preparation, PET-CT acqusition AK-H: manuscript preparation, target irradiation, dry distillation production process MSz: manuscript preparation, target irradiation MSo: manuscript preparation, concept discussion AdA: manuscript preparation, concept discussion. All authors read and approved the final manuscript.

Funding
Project was founded by internal statutory Grant No. DN/SN-07WP/19 at Maria Sklodowska-Curie National Research Institute of Oncology Gliwice Branch and partially supported by the Silesian University of Technology statutory research funds 02/040/BK_22/1022 (DB).

Availability of data and materials
Not applicable.

Declarations

Ethics approval and consent to participate
Not applicable.

Consent for publication
Not applicable.

Competing interests
Not applicable.

Author details
[1]Department of Nuclear Medicine and Endocrine Oncology, PET Diagnostics Unit, Maria Skłodowska-Curie National Research Institute of Oncology, Gliwice Branch, Gliwice, Poland. [2]Department of Systems Biology and Engineering, Silesian University of Technology, Akademicka 16, 44-100 Gliwice, Poland. [3]Biotechnology Center, Silesian University of Technology, Krzywoustego 8, 44-100 Gliwice, Poland. [4]Radiopharmacy and Preclinical PET Imaging Unit, Maria Skłodowska-Curie National Research Institute of Oncology, Gliwice Branch, Gliwice, Poland. [5]Department of Medical Physics, Maria Skłodowska-Curie National Research Institute of Oncology, Gliwice Branch, Gliwice, Poland.

Received: 8 November 2021 Accepted: 19 May 2022
Published online: 06 June 2022

References

1. Vaquero JJ, Kinahan P. Positron emission tomography: current challenges and opportunities for technological advances in clinical and preclinical imaging systems. Annu Rev Biomed Eng. 2015;17:385–414.
2. Happel C, Kranert WT, Ackermann H, Binse I, Bockisch B, Gröner D, Herrmann K, Grüwald F. Thyroid stunning in radioiodine-131 therapy of benign thyroid diseases. Endocrine. 2019;63:537–44.
3. Foss CA, Plyku D, Ordonez AA, Sanchez-Bautista J, Rosenthal HB, Il Minn, Lodge MA, Pomper MG, Sgouros G, Jain AK. Biodistribution and radiation dosimetry of 124 I-DPA-713, a PET radiotracer for macrophage-associated inflammation. J Nuclear Med. 2018;59:1751–6.
4. Kumar K, Ghosh A. Radiochemistry, production process, labeling, methods and immunoPET imaging pharmaceuticals of iodine-124. Molecules. 2021;26(2):414.
5. Hendrikse H, Kiss O, Kunikowska J, Wadsak W, Decristoforo C, Patt M. EANM position on the in-house preparation of radiopharmaceuticals. Eur J Nuclear Med Mol Imaging. 2022;1:1.
6. Cascini GL, Asabella AN, Notaristefano A, Restuccia A, Ferrari C, Rubini D, Altini C, Rubini G. ^{124}Iodine: a longer-life positron emitter isotope-new opportunities in molecular imaging. BioMed Res Int. 2014;1:5.
7. Pentlow KS, Graham MC, Lambrecht RM, Cheung NK, Larson SM. Quantitative imaging of I-124 using positron emission tomography with applications to radioimmunodiagnosis and radioimmunotherapy. Med Phys. 1991;18(3):357–66.

8. IAEA. Radioisotopes and Radiopharmaceuticals Reports No. 1. Cyclotron Produced Radionuclides: Emerging Positron Emitters for Medical Applications: 64Cu and 124I. 2016.
9. Koehler L, Gagnon K, McQuarrie S, Wuest F. Iodine-124: a promising positron emitter for organic PET chemistry. Molecules. 2010;15:2686–718.
10. Braghirolli AMS, Waissmann W, da Silva JB, Santos GR. Production of iodine-124 and its applications in nuclear medicine. Appl Radiat Isotopes. 2014;90:138–48.
11. Lambrecht RM, Sajjad M, Qureshi MA, Al Yanbawi SJ. Production of iodine-124. Radioanal Nucl Chem Lett. 1988;127:143–50.
12. Firouzbakht ML, Schlyer V, Finn RD, Laguzzi G, Wolf AP. Iodine-124 production: excitation functions for the 124Te(d,2n)124I and 124Te(d,3n)123I reactions from 7 to 24 MeV. Nucl Instrum Methods B. 1993;79:909–10.
13. Weinreich R, Knust EJ. Quality assurance of iodine-124 produced via the nuclear reaction Te-124(d,2n)I-124. Radioanal Nucl Chem Lett. 1996;213:253–61.
14. Clem RG, Lambrecht RM. Enriched Te-124 targets for production of I-123 and I-124. Nucl Instrum Methods Phys Res Sect A Accel Spectrom Detectors Assoc Equip. 1991;303:115–8.
15. Bastian T, Coenen HH, Qaim SM. Excitation functions of Te-124(d, xn)I- 124, I-125 reactions from threshold up to 14MeV:comparative evaluation of nuclear routes for the production of I-124. Appl Radiat Isot. 2001;55:303–8.
16. Sheh Y, Koziorowski J, Balatoni J, Lom C, Dahl JR, Finn RD. Low energy cyclotron production and chemical separation of "no carrier added" iodine-124 from a, reusable, enriched tellurium-124 dioxide. Radiochimica Acta. 2000;88(3):169.
17. Qaim SM, Hohn A, Bastian T, El-Azoney KM, Blessing G, Spellerberg S. Some optimization studies relevant to the production of high-purity I-124 and I-120g at a small-sized cyclotron. Appl Radiat Isot. 2003;58:49–78.
18. Glaser M, Mackay DB, Ranicar ASO, Waters SL, Brady F, Luthra SK. Improved targetry and production of iodine-124 for PET studies. Radiochem Acta. 2004;92:951–6.
19. Scholten B, Kovacs Z, Tarkanyi F, Qaim SM. Excitation functions of 124Te (p, xn)124, 123I reactions from 6 to 31 MeV with special reference to the production of 124I at a small cyclotron. Appl Radiat Isot. 1995;46:255–9.
20. IAEA. Technical Reports Series no. 468. Vienna, 2009.
21. Allison J, Amako K, Apostolakis J, Araujo H, Arce Dubois P, Asai M, Barrand G, Capra R, Chauvie S, Chytracek R, Cirrone GAP, Cooperman G, Cosmo G, Cuttone G, Daquino GG, Donszelmann M, Dressel M, Folger G, Foppiano F, Generowicz J, Grichine V, Guatelli S, Gumplinger P, Heikkinen A, Hrivnacova I, Howard A, Incerti S, Ivanchenko V, Johnson T, Jones F, Koi T, Kokoulin R, Kossov M, Kurashige H, Lara V, Larsson S, Lei F, Link O, Longo F, Maire M, Mantero A, Mascialino B, McLaren I, Mendez Lorenzo P, Minamimoto K, Murakami K, Nieminen P, Pandola L, Parlati S, Peralta L, Perl J, Pfeiffer A, Pia MG, Ribon A, Rodrigues P, Russo G, Sadilov S, Santin G, Sasaki T, Smith D, Starkov N, Tanaka S, Tcherniaev E, Tome B, Trindade A, Truscott P, Urban L, Verderi M, Walkden A, Wellisch JP, Williams DC, Wright D, Yoshida H. Geant4 developments and applications. IEEE Trans Nuclear Sci. 2006;53:270–8.
22. Allison J, Amako K, Apostolakis J, Arce P, Asai M, Aso T, Bagli E, Bagulya A, Banerjee S, Barrand G, Beck BR, Bogdanov AG, Brandt D, Brown JMC, Burkhardt H, Canal Ph, Cano-Ott D, Chauvie S, Cho K, Cirrone GAP, Cooperman G, Cortés-Giraldo MA, Cosmo G, Cuttone G, Depaola G, Desorgher L, Dong X, Dotti A, Elvira VD, Folger G, Francis Z, Galoyan A, Garnier L, Gayer M, Genser KL, Grichine VM, Guatelli S, Guèye P, Gumplinger P, Howard AS, Hřivnáčová I, Hwang S, Incerti S, Ivanchenko A, Ivanchenko VN, Jones FW, Jun SY, Kaitaniemi P, Karakatsanis N, Karamitrosi M, Kelsey M, Kimura A, Koi T, Kurashige H, Lechner A, Lee SB, Longo F, Maire M, Mancusi D, Mantero A, Mendoza E, Morgan B, Murakami K, Nikitina T, Pandola L, Paprocki P, Perl J, Petrović I, Pia MG, Pokorski W, Quesada JM, Raine M, Reis MA, Ribon A, Ristić Fira A, Romano F, Russo G, Santin G, Sasaki T, Sawkey D, Shin JI, Strakovsky II, Taborda A, Tanaka S, Tomé B, Toshito T, Tran HN, Truscott PR, Urban L, Uzhinsky V, Verbeke JM, Verderi M, Wendt BL, Wenzel H, Wright DH, Wright DM, Yamashita T, Yarba J, Yoshida H. Recent developments in GEANT4. Nuclear Inst Methods Phys Res. 2016;835:186–225.
23. ...Agostinelli S, Allison J, Amako K, Apostolakis J, Araujo H, Arce P, Asai M, Axen D, Banerjee S, Barrand G, Behner F, Bellagamba L, Boudreau J, Broglia L, Brunengo A, Burkhardt H, Chauvie S, Chuma J, Chytracek R, Cooperman G, Cosmo G, Degtyarenko P, Dell'Acqua A, Depaola G, Dietrich D, Enami R, Feliciello A, Ferguson C, Fesefeldt H, Folger G, Foppiano F, Forti A, Garelli S, Giani S, Giannitrapani R, Gibin D, Gómez Cadenas JJ, González I, Gracia Abril G, Greeniaus G, Greiner W, Grichine V, Grossheim A, Guatelli S, Gumplinger P, Hamatsu R, Hashimoto K, Hasui H, Heikkinen A, Howard A, Ivanchenko V, Johnson A, Jones FW, Kallenbach J, Kanaya N, Kawabata M, Kawabata Y, Kawaguti M, Kelner S, Kent P, Kimura A, Kodama T, Kokoulin R, Kossov M, Kurashige H, Lamanna E, Lampén T, Lara V, Lefebure V, Lei F, Liendl M, Lockman W, Longo F, Magni S, Maire M, Medernach E, Minamimoto K, Mora de Freitas P, Morita Y, Murakami K, Nagamatu M, Nartallo R, Nieminen P, Nishimura T, Ohtsubo K, Okamura M, O'Neale S, Oohata Y, Paech K, Perl J, Pfeiffer A, Pia MG, Ranjard F, Rybin A, Sadilov S, Di Salvo E, Santin G, Sasaki T, Savvas N, Sawada Y, Scherer S, Sei S, Sirotenko V, Smith D, Starkov N, Stoecker H, Sulkimo J, Takahata M, Tanaka S, Tcherniaev E, Safai Tehrani E, Tropeano M, Truscott P, Uno H, Urban L, Urban P, Verderi M, Walkden A, Wander W, Weber H, Wellisch JP, Wenaus T, Williams DC, Wright D, Yamada T, Yoshida H, Zschiesche D, GEANT4 Collaboration. GEANT4-a simulation toolkit. Nuclear Inst Methods Phys Res. 2003;506:250–303.
24. Ziegler JF. Interactions of ions with matter 2013. http://www.srim.org/. Accessed 12 May 2021.
25. Poignant F, Penfold S, Asp J, Takhar P, Jackson P. GEANT4 simulation of cyclotron radioisotope production in a solid target. Physica Medica. 2016;32(5):728–34.
26. Poniger SS, Tochon-Danguy HJ, Panopoulos HP, O'Keefe GJ, Peake D, Rasool R, Scott AM. Automated production of 124I and 64Cu using IBA Terimo and Pinctada metal electroplating and processing modules. AIP Conf Proc. 2012;1509:114–9.
27. Tagiara NS, Palles D, Simandiras ED, Psycharis V, Kyritsis A, Kamitsos EI. Synthesis, thermal and structural properties of pure TeO_2 glass and zinc-tellurite glasses. J Non-Cryst Solids. 2017;457:116–25.
28. Marple MAT, Jesuit M, Hung I, Gan Z, Feller S, Sen S. Structure of TeO2 glass: results from 2D 125Te NMR spectroscopy. J Non-Cryst Solids. 2019;513:183–90.
29. IAEA. Charged particle cross-section database for medical radioisotope production: diagnostic radioisotopes and monitor reactions Final report of a co-ordinated research project. 2001.
30. Alternative Radionuclide Production with a Cyclotron. Number 4 in Radioisotopes and Radiopharmaceuticals Reports. INTERNATIONAL ATOMIC ENERGY AGENCY, Vienna, 2021.

31. European Pharmacopoeia 10th edition Volume I Implementation: 01/2020. The European Directorate for the Quality of Medicines & HealthCare (EDQM).
32. Saha GB. Quality control of radiopharmaceuticals. Cham: Springer International Publishing; 2018. p. 163–83.
33. Joseph CH. Chapter 14: Quality control of radiopharmaceuticals. In: Radiopharmaceuticals in nuclear pharmacy and nuclear medicine, 4th Edition, 2020.
34. Balatoni J, Finn R, Blasberg R, Tjuvajev J, Larson S. Production and quality assurance of cyclotron produced iodine-124 from enriched tellurium targets. In: The fifteenth international conference on the application of accelerators in research and industry. AIP Conference Proceedings, vol 475, pp 984–986 (1999).
35. Turner JE. Atoms, radiation, and radiation protection. New York: Wiley; 1995.
36. Jentzen W, Richter M, Nagarajah J, Poeppel TD, Brandau W, Dawes C, Bockisch A, Binse I. Chewing-gum stimulation did not reduce the absorbed dose to salivary glands during radioiodine treatment of thyroid cancer as inferred from pre-therapy ^{124}I PET/CT imaging. EJNMMI Phys. 2014;1:100.
37. Fanchon LM, Beattie BJ, Pentlow K, Larson SM, Humm JL. Optimizing reconstruction parameters for quantitative ^{124}I-PET in the presence of therapeutic doses of ^{131}I. EJNMMI Phys. 2021;8:50.
38. Jentzen W, Phaosricharoen J, Gomez B, Hetkamp P, Stebner V, Binse I, Kinner S, Herrmann K, Sabet A, Nagarajah J. Quantitative performance of ^{124}I PET/MR of neck lesions in thyroid cancer patients using ^{124}I PET/CT as reference. EJNMMI Phys. 2018;5:13.
39. Kersting D, Jentzen W, Sraieb M, Costa PF, Conti M, Umutlu L, Antoch G, Herrmann K, Nader M, Fendler WP, Rischpler C, Weber M. Comparing lesion detection efficacy and image quality across different PET system generations to optimize the iodine-124 PET protocol for recurrent thyroid cancer. EJNMMI Phys. 2021;8:14.
40. Roelcke U, Hausmann O, Merlo A, Missimer J, Maguire RP, Freitag P, Radü EW, Weinreich R, Gratzl O, Leenders KL. PET imaging drug distribution after intratumoral injection: the case for 124-I. J Nucl Med. 2002;43:1444–51.
41. Pentlow KS, Graham MC, Lambrecht RM, Daghighian F, Bacharach SL, Bendriem B, Finn RD, Jordan K, Kalaigian H, Karp JS, Robeson WR, Larson SM. Quantitative imaging of Iodine-124 with PET. J Nucl Med. 1996;37:1557–62.
42. Freudenberg LS, Antoch G, Jentzen W, Pink R, Knust J, Görges R, Mülle SP, Bockisch A, Debatin JF, Brandau W. Value of 124I-PET/CT in staging of patients with differentiated thyroid cancer. EurRadiol. 2004;14:2092–8.
43. Lubberink M, Herzog H. Quantitative imagining of ^{124}I and ^{86}Y. Nuclear Med Mol Imaging (2011).
44. Vandenberghe S. Three-dimensional positron emission tomography imaging with 124I and 86Y. Nucl Med Commun. 2006;27:237–45.
45. Synowiecki MA, Perk LR, Nijsen FW. Production of novel diagnostic radionuclides in small medical cyclotrons. EJNMMI Radiopharm Chem. 2018;3:3.
46. George KJH, Borjian S, Cross MC, Hicks JW, Schaffer P, Kovacs MS. Expanding the PET radioisotope universe utilizing solid targets on small medical cyclotrons. RSC Adv. 2021;11:31098–123.
47. Marin JFG, Nunes RF, Coutinho AM, Zaniboni EC, Costa LB, Barbosa FG, Queiroz MA, Cerri GG, Buchpiguel CA. Theranostics in nuclear medicine: emerging and re-emerging integrated imaging and therapies in the era of precision oncology. Radiographics. 2020;6(40):1715–40.
48. Pham TT, Lu Z, Davis Ch, Li Ch, Sun F, Maher J, Yan R. Iodine-124 based dual positron emission tomography and fluorescent labeling reagents for in vivo cell tracking. Bioconjug Chem. 2020;31(4):1107–16.
49. Gharibkandi NA, Gierałtowska J., Wawrowicz K., Bilewicz A,. Nanostructures as radionuclide carriers in auger electron therapy. Materials. 2022;15(3):1143.
50. Nikjoo H, Emfietzoglou D, Charlton DE. The Auger effect in physical and biological research. Int J Radiat Biol. 2008;84(12):1011–26.
51. Ku A, Facca VJ, Cai Z, Reilly RM. Auger electrons for cancer therapy–a review. EJNMMI Radiopharmacy Chem. 2019;4(1):27.
52. Falzone N, Fernández-Varea JM, Flux G, Vallis KA. Monte carlo evaluation of auger electron-emitting theranostic radionuclides. J Nuclear Med. 2015;56(9):1441–6.
53. Turner JH. An introduction to the clinical practice of theranostics in oncology. Br J Radiol. 2018;91(1091):20180440.
54. Qaim SM, Scholten B, Neumaier B. New developments in the production of theranostic pairs of radionuclides. J Radioanal Nuclear Chem. 2018;318(3):1493–509.
55. Barca C, Griessinger CM, Faust A, Depke D, Essler M, Windhorst AD, Devoogdt N, Brindle KM, Schäfers M, Zinnhardt B, Jacobs AH. Expanding theranostic radiopharmaceuticals for tumor diagnosis and therapy. Pharmaceuticals (Basel, Switzerland). 2021;15(1):12.
56. Comora JJ, Stevanovic Z, Rajcevic M, Kosutic D. Modeling of thermal properties of a TeO_2 target for radioiodine production. Nucl Inst Methods Phys Res A. 2004;521:161–70.
57. Fonslet J, Koziorowski J. Dry distillation of radioiodine from TeO_2 targets. Appl Sci. 2013;5:10.
58. Rovais MRA, Yousefi K, Ardaneh K, Mirzaii M. Computer simulation of temperature distribution on a solid target for 201Tl production. Nukleonika. 2011;56(4):283–9.
59. Azizakram H, Sadeghi M, Ashtari P, Zolfagharpour F. A Monte Carlo approach to calculate the production prerequisites of 124I radioisotope towards the activity estimation. Nuclear Technol Radiat Protect. 2018;33(1):68–74.
60. Sadeghi M, Enferadi M, Ensaf M. ^{124}I production for PET imaging at a cyclotron. Kerntechnik. 2012;77:10.
61. Nagatsu K, Fukada M, Minegishi K, Suzuki H, Fukumura T, Yamazaki H, et al. Fully automated production of iodine-124 using a vertical beam. Radiat Isotopes. 2011;69:146–57.
62. Schmitz J. The production of I-124 iodine and Y-86 yttrium. Mol Imaging. 2011;38:4–9.
63. Hussein AA, Jarallah NT, Saied BM. Evaluation the reactions of production the radioactive Iodine-124. J Phys Conf Ser. 2021;1879:032107.

Publisher's Note